

# Theoretical Investigation of 2D Conductive Microporous Coordination Polymers as Li–S Battery Cathode with Ultrahigh Energy Density

Guoping Gao, Fan Zheng, Feng Pan, and Lin-Wang Wang\*

Even though tremendous achievement has been made experimentally in the performance of lithium–sulfur (Li–S) battery, theoretical studies in this area are lagging behind due to the complexity of the Li–S systems and the effects of solvent. For this purpose, a new methodology is developed for investigating the 2D hexaaminobenzene-based coordination polymers (2D-HAB-CPs) as cathode candidate materials for Li–S batteries via density functional theory calculations in combination with an in-house developed charge polarized solvent model and a genetic algorithm structure global search code. With high ratios of transition metal atoms and two-coordinated nitrogen atoms, excellent electric conductivity, and structural porosity, the 2D-HAB-CP is able to address all of the three main challenges facing Li–S batteries: confining the lithium polysulfides from dissolution, facilitating the electron conductivity and buffering the volumetric expansion during the lithiation process. In addition, the theoretical energy density of this system is as high as  $1395 \text{ Wh kg}^{-1}$ . These results demonstrate that the 2D-HAB-CP is a promising cathode material for Li–S batteries. The proposed computational framework not only opens a new avenue for understanding the key role played by solution and liquid electrolytes in Li–S batteries, but also can be generally applied to other processes with liquids involved.

transition-metal oxide (LTMO)/phosphate cathodes that intercalating Li ions with the minimal structural change due to the nature of intercalation and stabilities of the LTMO. However, the same factors also fundamentally limit its energy density.<sup>[1]</sup> The current LIB cathodes can reach an energy density of about  $300 \text{ Wh kg}^{-1}$ , which is close to their theoretical limit.<sup>[2]</sup> The intercalation happens by Li donates its electron to the host while the transition metal (TM) atoms change their covalence states to accommodate the extra electron. Since this is more like the ionic interaction with no direct Li-transition metal bonding, the Li can often diffuse inside such LTMO. Nevertheless, noncovalent bonding also means weak binding strength and low energy density. To go beyond LIB, the community has worked on nonintercalation based battery.<sup>[2]</sup> The rechargeable lithium–sulfur (Li–S) battery is intensely studied for this purpose. Its theoretical energy density is  $2567 \text{ Wh kg}^{-1}$ , which is 3–5 times higher than those of state-of-art LIBs.<sup>[3]</sup> In addition, sulfur is cheap, earth-

abundant, nontoxic, and environmental friendly element.<sup>[4]</sup> Unlike the LIBs, the Li–S battery works by the formation of chemical bonds between Li and S. Such bonds are weaker compared with Li–O bonds in the lithium air battery; hence, it has smaller theoretical energy density than the lithium air battery,<sup>[3,5]</sup> but at the same time, the Li–S reaction it is easier to manage and control compared to Li–O reaction. Thus, Li–S battery presents a compromise, which can serve as the first step to go beyond the LIBs. Given all these promises, there are however tremendous scientific and technical challenges which have hindered the commercialization of Li–S batteries<sup>[6]</sup>: I) The shuttling effect stemming from the soluble lithium polysulfides ( $\text{Li}_2\text{S}_\gamma$ ,  $4 \leq \gamma \leq 8$ ), which causes the loss of active materials and rapid capacity fading. The intermediate lithiation states are completely soluble, and actually they can only sustain their voltages in the solvated states. This will cause the  $\text{Li}_2\text{S}_\gamma$  to be decomposed on the Li metal anode and to lose capacity of the system; II) the insulating nature of both sulfur and the final reduction product  $\text{Li}_2\text{S}$ , which impedes the lithiation process; and III) the 80% volumes change during cycling process, which causes structural damage and mechanical instability. One common method to address II) and III) is to use highly

## 1. Introduction

Lithium-ion batteries (LIBs) are an integrated part of our daily life used in cell phone, laptop computers, and hybrid vehicle. The LIBs are composed of graphite anodes and Li

Dr. G. Gao, Prof. L.-W. Wang  
Materials Sciences Division  
Lawrence Berkeley National Laboratory  
Berkeley, CA 94720, USA  
E-mail: lwwang@lbl.gov

Dr. F. Zheng  
Joint Center for Artificial Photosynthesis  
Lawrence Berkeley National Laboratory  
Berkeley, California 94720, USA

Prof. F. Pan  
School of Advanced Materials  
Peking University  
Shenzhen Graduate School  
Shenzhen 518055, P. R. China

 The ORCID identification number(s) for the author(s) of this article can be found under <https://doi.org/10.1002/aenm.201801823>.

DOI: 10.1002/aenm.201801823

mesoporous conducting hosts to introduce electric conductivity and to buffer the volume change. For this purpose, the conductive porous carbon materials<sup>[7]</sup> are often used. However, the weak interaction between nonpolar carbon and pure sulfur or  $\text{Li}_2\text{S}_y$  make it difficult to be used as an adhesive material to prevent Li-polysulfide dissolution (challenge I).<sup>[8]</sup> To address this challenge, sometimes cage-like electrodes are used to physically encapsulate S molecules and clusters.<sup>[9]</sup> However, such physical encasement is difficult to realize and to be made stable.<sup>[10]</sup> Another possibility is to bind the  $\text{Li}_2\text{S}_y$  to a metal oxide substrate with strong adhesion,<sup>[11]</sup> so it will be prevented from dissolution thermodynamically. The key is to keep the high-energy density despite the added weight of the substrate and the strong binding to the substrate. In this regard, the bulk substrate with small surface/volume ratio will be too heavy,<sup>[11a]</sup> thus 2D substrates or frameworks will be beneficial. Another advantage of using a 2D substrate is to provide electric conductivity.<sup>[12]</sup> On the other hand, transition metal can be used as an anchoring point for pure sulfur and  $\text{Li}_2\text{S}_y$ . For this regard, porous metal-organic framework (MOF) materials have been used.<sup>[13]</sup> Unfortunately, the MOF does not provide the necessary electric conductivity, thus some other electric binders must be added, which increase the complexity of the system.<sup>[14]</sup> What needed is a system, which is 2D, or 3D porous structure, contains transition metals and is also electrically conductive. Recently, a new class of material named 2D coordination polymer: 2D hexaaminobenzene-based coordination polymers (2D-HAB-CPs), has been synthesized.<sup>[15]</sup> It consists of transition metal coordinately bonded with a small unit of conjugated polymer formed by C and N elements. Unlike the MOF, this system is electrically conductive, thus it satisfies the above criterions, combining the merits of both the porous carbon materials and MOFs as the Li-S battery cathode.<sup>[15,16]</sup> More excitingly, Bao and co-workers have experimentally proved that the 2D-HAB-CP can exhibit high volumetric and areal capacitance as a Li-cathode material.<sup>[17]</sup> However, that work used the 2D-HAB-CP as it is, without the addition of S. Thus it is not a sulfur battery, and the energy density is relatively low. In the present work, we will theoretically investigate the use of 2D-HAB-CP as a Li-S battery cathode by adding sulfur atoms on the substrate.

Even though tremendous achievement has been made experimentally in the performance of Li-S battery, theoretical studies in this area are lagging behind.<sup>[18]</sup> Part of the reason is the complexity of the Li-S systems. Unlike the LIBs, which happen in the crystal structure, the Li-S reactions have much more complex configurations. Direct first principle molecular dynamics simulation cannot be run long enough to direct simulate the reaction process. Thus, one has to search for the global minimum structures. The effects of solvent further complicate the issue.<sup>[19]</sup>  $\text{Li}^+$  is a highly polarizable ion, with strong ion-solvent interaction energy. Some of the commonly available solvent models diverge in this system. This makes it difficult even to study the energies of the isolated  $\text{Li}_2\text{S}_y$  molecule in the solvent. In this work, we developed an ab initio approach based on density functional theory (DFT) to study the Li-S battery energetics on 2D-HAB-CP substrate. At first, specific ion-solvent interaction parameters are developed for our continuum solvent model based on the experimental discharging voltage data for the  $\text{Li}_2\text{S}_y$  molecule in the electrolyte.

Then the global minimum configurations are searched through an in-house developed genetic algorithm search code for the structure of  $\text{Li}_2\text{S}_y$  on top of 2D-HAB-CP. The reaction energetics is analyzed based on the DFT calculations. We found that the transition metal atoms in 2D-HAB-CP can effectively capture the sulfur atoms, while the two-coordinated nitrogen edges atoms are preferred sites for Li binding during the charge/discharge process. With sufficient Lithium, the system demonstrates a layer structure with alternating Li and S atoms, which resemble that of the bulk  $\text{Li}_2\text{S}$ . The highest energy density is about  $1395 \text{ Wh kg}^{-1}$ . Besides, the 2D-HAB-CP can significantly reduce the dissolution of  $\text{Li}_2\text{S}_y$ , although it does not completely block it on the thermodynamic ground. Perhaps a changing of the transition metal like V or Cr can further improve this aspect.<sup>[6a,20]</sup> Finally, the system shows excellent electric conductivity throughout the lithiation process. As for the volumetric change of the system, we have introduced a 2D-HAB-CP/S/2D-HAB-CP sandwich structure. Preliminary tests show that its volume change during lithiation is as small as 3%, rivals that in LIB.

## 2. Computation Details

All calculations were performed using DFT coded in the PWmat code.<sup>[21]</sup> The exchange-correlation interactions were treated by the generalized gradient approximation<sup>[22]</sup> in the form of the Perdew-Burke-Ernzerhof functional.<sup>[23]</sup> The Van der Waals interaction was described by using the empirical correction in Grimme's scheme, i.e.  $\text{DFT}+\text{D}_2$ .<sup>[24]</sup> The spin = 2 polarization was used in all the calculations. The electron wave functions were expanded by plane waves with cut-off energies of 680 eV, and the convergence tolerance for residual force and energy on each atom during structure relaxation were set to  $0.005 \text{ eV \AA}^{-1}$  and  $10^{-5} \text{ eV}$ , respectively. The vacuum space was more than  $20 \text{ \AA}$  to avoid the interaction between periodical images. The Hubbard U (DFT+U) treatment was used on the transition metal. The U value for Mn was set to 3.06 eV following the literature value.<sup>[25]</sup> The solvent effects were simulated with implicit charge polarizable solvent model,<sup>[26]</sup> which uses fixed ion charge to define the onsite of the dielectric function. We found that the self-consistent continuum solvation model model<sup>[27]</sup> was difficult to converge for the case of Li. The solvent dielectric constant used in the solvent model is fit to be 7.8 to simulate the solvent effects of 1,2-dimethoxyethane(DME)/1,3-dioxolane(DOL) (1: 1, v: v). The choice of other solvent model parameters will be discussed later. The model is efficient to include approximate solvent effects where the solvent is not an active constituent in the reaction or process.<sup>[28]</sup> So, no explicit solvent molecules are present in our calculation. For crystal calculations, the solvent model should not be used. More details of free energy calculation can be found in the Supporting Information. In the solvent, the adsorption energy of polysulfide is defined by following Equation (1):

$$E_{\text{ads}} = E_{\text{polysulfide}^*}(\text{aq}) - E^*(\text{aq}) - E_{\text{polysulfide}}(\text{aq}) \quad (1)$$

Here, \* represents the Mn-HAB-CP, and aq is the solvent effects (with solvent molecule surrounding the whole system) is included in our solvent model.

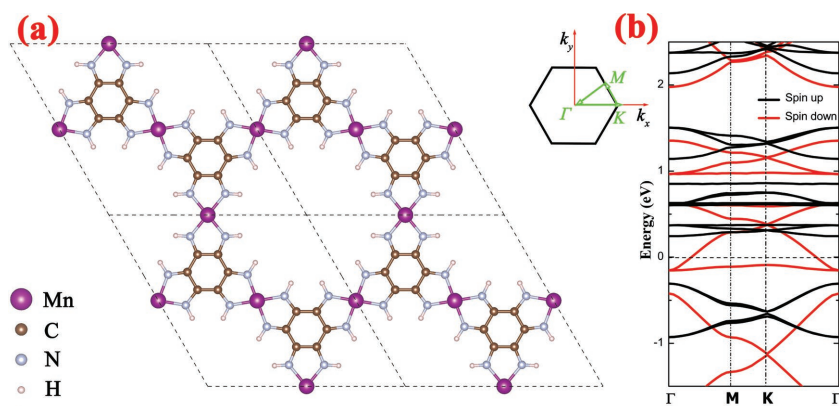


**Figure 1.** a) The geometric structure of Mn-HAB-CP monolayer. b) The band structure of Mn-HAB-CP monolayer along the high symmetry  $\Gamma$ -K-M- $\Gamma$  directions and the associated Brillouin zone. The Fermi energy in the band structure is at 0.

### 3. Results

**Figure 1a** presents the configuration of the 2D-HAB-CP, which has been synthesized using the “bottom-up” method.<sup>[15]</sup> The stability of it was tested by ab initio molecular dynamics simulation at 300K for about 1000 fs. As shown in Figure S5 in the Supporting Information, although there is some small warping, the overall structure is intact. We believe this shows the stability of the synthesized 2D-HAB-CP, confirming the experimental synthesis of this material. The unit cell of 2D HAB-CP consists of three equivalent TM atoms (linkers) in a hexagonal honeycomb lattice. Each TM atom is surrounded by four N atoms forming a square planar arrangement of nitrogen-coordinated metal macrocycles. Based on our initial calculation, the interaction between  $S_8$  and transition metal will weaken with the number of *d*-electrons and the late transition metals, such as Zn, cannot capture the  $S_8$  firmly which is confirmed by previous work as well.<sup>[29]</sup> On the other side, the 2D hexaaminobenzene-based coordination polymers with early transition metal atoms, like Sc or Ti, cannot maintain metallic nature due to the lack of spare *d*-electrons for *d*-*p*- $\pi$  conjugation. Therefore, Mn, in the middle of the transition metals, is chosen as the compromise TM linker to investigate the potential of Mn-HAB-CP in the Li-S batter application. The metallic nature of Mn-HAB-CP, due to the effects of *d*-*p*- $\pi$  conjugation, is confirmed by the no-gap band structure shown in Figure 1b. The band structure has a relatively large dispersion at the Fermi energy, which indicates band-like charge transport, instead of localized state hopping.

Before the calculation of Li polysulfides binding with the substrate, it is necessary to first study the Gibbs-free formation energy of the  $Li_2S_\gamma$  molecules in the electrolyte. In the experiment, the Li-S battery operator in the in electrolyte solvents, such as DME or DOL. One of the problems of Li-S battery, the shuttle effect, is caused by the dissolution of lithium polysulfide ( $Li_2S_\gamma$ ,  $4 \leq \gamma \leq 8$ ) in the solvent. However, it is a long-standing challenge to theoretically predict the solvent behaviors of polysulfide and to calculate the solvated Gibbs formation energies of these polysulfide.<sup>[19,30]</sup> In our calculation, the charge polarizable solvent model with a fixed ion charge to determine the dielectric function profile is used to represent the solvent

effect. Nevertheless, the onsite distance of the dielectric screening from the Li nuclear is a critical parameter which determines the solvation energy. Unfortunately, at this stage, direct ab initio calculation with the default parameter for the solvation model does not provide accurate solvation energy. To solve this problem, we have used experimental results to fix our solvent model parameter. Experimentally, the charging/discharging voltages for the stage from  $S_8$  to  $Li_2S_4$  are known. Since the  $Li_2S_\gamma$  ( $4 \leq \gamma \leq 8$ ) is dissolved in the solvent as molecules, these charging voltages effectively provide the Gibbs-free formation energies of these molecules in the electrolyte (The conversion method between calculated Gibbs-free formation energies and experimental voltage can be found in Section 2 in the Supporting Information).

We can thus adjust our solvent model parameter to reproduce the experimental curve.<sup>[31]</sup> Note that, the states of Li,  $Li_2S$ ,  $Li_2S_2$ , and  $S_8$  are all in solid crystal form, thus there is no solvent effect. As a fit, we have chosen an ion-charge induced dielectric profile parameter of 7.8 in the PWmat implementation in order for our solvent model to agree with the experiment as shown in **Figure 2**. The induced polarization charges of  $Li_2S_\gamma$  ( $4 \leq \gamma \leq 8$ ) are shown in Figure S1 in the Supporting Information. The experimental formation energies converted from the experimental charging/discharging voltages<sup>[4b,31]</sup> are shown in Figure 2 as the dashed line. We find that the experimental formation energy of final production (bulk  $Li_2S$ ,  $-1.47$  eV per atom) can be obtained by the most stable  $\alpha$ -octasulfur and Li crystal structures<sup>[5]</sup> [ $\frac{1}{8}S_8(s) + Li(s) \rightarrow Li_2S(s)$ ]. There are some debates for the existence of  $Li_2S_2$  and its structure in the solvent.<sup>[32]</sup> Using the fitted solvent model parameter, the formation energy of one  $Li_2S_2$  molecule in the solvent is only  $-0.74$  eV per atom, far higher from the experimental value ( $-1.14$  eV per atom). We also

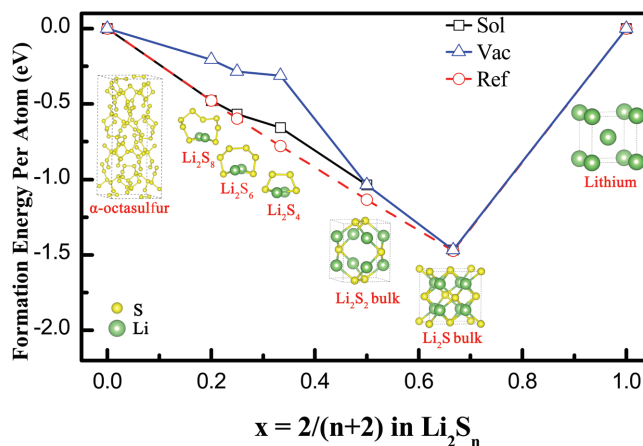


**Figure 2.** The computational Gibbs-free formation energies of some key polysulfide per atom involved in different lithiation stages in the vacuum (black line) and DME/DOL (v:v, 1:1) electrolyte (blue line). The experimental formation energies converted from the experimental charging/discharging voltages are present in the red dash line as a reference.

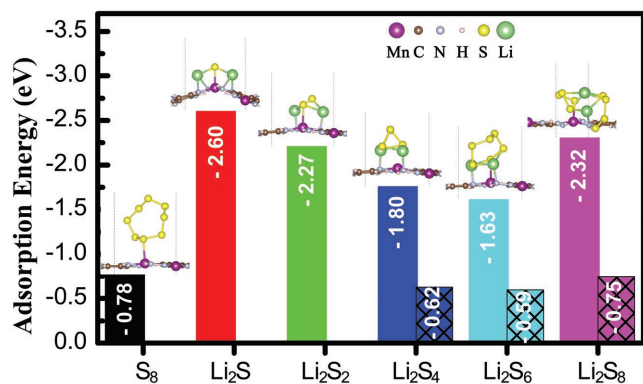


**Figure 3.** The adsorption energy of isolated S<sub>8</sub>, and Li<sub>2</sub>S<sub>γ</sub> molecule on Mn-HAB-CP in the vacuum (bars without patterns) and solvent (bars with net pattern).

find that, no matter what parameter we use, we cannot obtain a good fit of Li<sub>2</sub>S<sub>2</sub> energy to the experiment if it exists as a dissolved molecule. On the other hand, if the bulk crystal structure as predicted by Yang et al.<sup>[33]</sup> is used for Li<sub>2</sub>S<sub>2</sub>, the formation energy will be  $-1.04$  eV per atom  $\frac{1}{4}S_8(s) + Li(s) \rightarrow Li_2S_2(s)$ , which is close to the experimental value. This can be viewed as a peripheral proof the Li<sub>2</sub>S<sub>2</sub> should exist as a crystal or large cluster in the solvent, consistent with the conclusion of a recent molecular dynamics simulation.<sup>[32b,34]</sup> For Li<sub>2</sub>S<sub>4</sub>, Li<sub>2</sub>S<sub>6</sub> and Li<sub>2</sub>S<sub>8</sub> clusters  $\frac{\gamma}{8}S_8(s) + Li(s) \rightarrow Li_2S_\gamma(aq), 4 \leq \gamma \leq 8$ , the formation energy in the vacuum can be higher than that of the experimental values by 0.5 eV per atom indicating the importance of the solvation energy. After including the solvent effects, the biggest difference between the theoretically predicted formation energy and the experiment is about 0.1 eV per atom. The overall agreement between experiment and theory is good, in line with the general accuracy of the DFT calculations.

Haven fixed the solvent model, we can now estimate the binding of Li<sub>2</sub>S<sub>γ</sub> ( $4 \leq \gamma \leq 8$ ) to the Mn-HAB-CP in the solvent. We have calculated the Li<sub>2</sub>S, Li<sub>2</sub>S<sub>2</sub> and S<sub>8</sub> binding on Mn-HAB-CP in the vacuum environment, while Li<sub>2</sub>S<sub>γ</sub> ( $4 \leq \gamma \leq 8$ ) in both solvent and vacuum environments (Figure 3). The S<sub>8</sub> molecule binds on top of one Mn atom with an adsorption energy of  $-0.78$  eV, indicating that it can be absorbed and melt on the Mn-HAB-CP substrate due to the existence of the transition metal. It was found that, in pure carbon nitride 2D systems, the S<sub>8</sub> will not bind to the substrate.<sup>[32a]</sup> For Li<sub>2</sub>S, the S atom is bind on the Mn site, while each Li atom is grasped firmly by two nitrogen atom. The adsorption energy of Li<sub>2</sub>S molecular on Mn-HAB-CP is as high as  $-2.60$  eV, which is  $-1.46$  eV stronger than it on graphene (see Figure S2 in the Supporting Information) and comparable with that on 2D transition metal disulfides.<sup>[35]</sup> The other polysulfides also show similar adsorption behavior on Mn-HAB-CP and exhibit strong binding strength. The adsorption energies of Li<sub>2</sub>S<sub>4</sub>, Li<sub>2</sub>S<sub>6</sub>, and Li<sub>2</sub>S<sub>8</sub> are  $-1.80$ ,  $1.63$ , and  $-2.32$  eV respectively when measured in vacuum. In the solvent, the bonding distance of polysulfides from the Mn and N anchoring atoms increase slightly and the adsorption energies reduce to  $-0.62$ ,  $-0.59$ , and  $-0.75$  eV for

Li<sub>2</sub>S<sub>4</sub>, Li<sub>2</sub>S<sub>6</sub>, and Li<sub>2</sub>S<sub>8</sub>, respectively. These negative adsorption energy values indicate that the polysulfides prefer to be adsorbed on the Mn-HAB-CP rather than being extricated in the solvent. Therefore, the high ratios of both Mn and N atoms in Mn-HAB-CP enable it as a bifunctional host for lithium polysulfide, which not only captures and but also electrically activates the insulating S<sub>8</sub>.

To further study the lithiation process, we first place one S<sub>8</sub> molecular per unit cell on Mn-HAB-CP then gradually add Li atoms to the cluster to form Li<sub>x</sub>S<sub>8</sub> until 20 lithium atoms have been added. The global energy minimum structures of Li<sub>x</sub>S<sub>8</sub> binding to the 2D coordination polymers are obtained using our in-house code, which implements the genetic algorithm to find the global minimum.<sup>[36]</sup> For each generation, the DFT relaxation of the populations is performed with PWmat. The process of our global minimum structure search code is present in the Figure S3 in the Supporting Information. The global energy minimum configurations are shown in Figure 4a–t. In the beginning, when there is no Li atom, the S<sub>8</sub> is attached to the Mn as shown in Figure 3. The first lithium atom opens the S<sub>8</sub> ring with one S atom binding on a Mn atom and the Li atom binding on a nitrogen atom (LiS<sub>8</sub>, see Figure 4a). With the second lithium added, the Li<sub>2</sub>S<sub>8</sub> cluster is in a dumbbell shape with two S<sub>4</sub> isomers at each end. The third added lithium will bridge between the end of one S<sub>4</sub> isomer of Li<sub>3</sub>S<sub>8</sub> and two nitrogen atoms of Mn-HAB-CP (Li<sub>3</sub>S<sub>8</sub>, see Figure 4c). In the Li<sub>4</sub>S<sub>8</sub> and Li<sub>5</sub>S<sub>8</sub>, the S<sub>4</sub> isomers are divided by lithium atoms into smaller ones, like S<sub>2</sub>, and S<sub>3</sub>. With more than six lithium atoms, Li<sub>x</sub>S<sub>8</sub> ( $6 \leq x \leq 11$ ) forms parallel 1D wires. The S isomers larger than S<sub>2</sub> disappear. When the lithium number is larger than 11, the 1D Li<sub>x</sub>S<sub>8</sub> wires interweave into a 2D three-layers-sandwich like structure: two lithium layers and one sulfur layer. The S<sub>2</sub> dimmers observed in earlier structures are melting into isolated S atoms gradually forming the middle layer of the sandwich framework with two layers of lithium atoms exposed (see Figure S5 in the Supporting Information). One lithium layer attaches to the Mn-HAB-CP firmly and there is no Mn-S binding remaining.

The above configurations only consider Li<sub>x</sub>S<sub>8</sub> at one side of Mn-HAB-CP. In reality, both sides can attach Li<sub>x</sub>S<sub>8</sub> simultaneously. To study that, we have added another Li<sub>16</sub>S<sub>8</sub> cluster on the other side of the Mn-HAB-CP-Li<sub>20</sub>S<sub>8</sub> structure to fully explore the Li–S battery potential. This Li<sub>16</sub>S<sub>8</sub> cluster forms another 2D sandwich framework on the other side of Mn-HAB-CP (see Figure 4u,v). We do find that, if Li<sub>20</sub>S<sub>8</sub> is added to the other side of Mn-HAB-CP-Li<sub>20</sub>S<sub>8</sub>, the structure becomes unstable.

Figure 5a plots the formation energy of Li<sub>x</sub>S<sub>8</sub> on Mn-HAB-CP as a function of the number of Li in the solvent. The formation energy is calculated as in following:

$$E_{\text{form}} = E_{\text{Li}_x\text{S}_8^*} - E_{\text{S}_8^*} - xE_{\text{Li bulk per atom}} \quad (2)$$

Here,  $E_{\text{Li}_x\text{S}_8^*}$ , and  $E_{\text{S}_8^*}$  are the total energy of Li<sub>x</sub>S<sub>8</sub> on Mn-HAB-CP, and S<sub>8</sub> on Mn-HAB-CP calculated in the solvent, respectively.  $E_{\text{Li bulk per atom}}$  is the energy per Li atom in its bulk form. Remarkable, the formation energy of Li<sub>x</sub>S<sub>8</sub> is almost a linear line of the number of Li. The linear formation energy as a function of the lithium atom indicates a constant voltage ( $1.74$  V) during the charge and discharge process, a very good feature and a significant advantage compared to other cathode

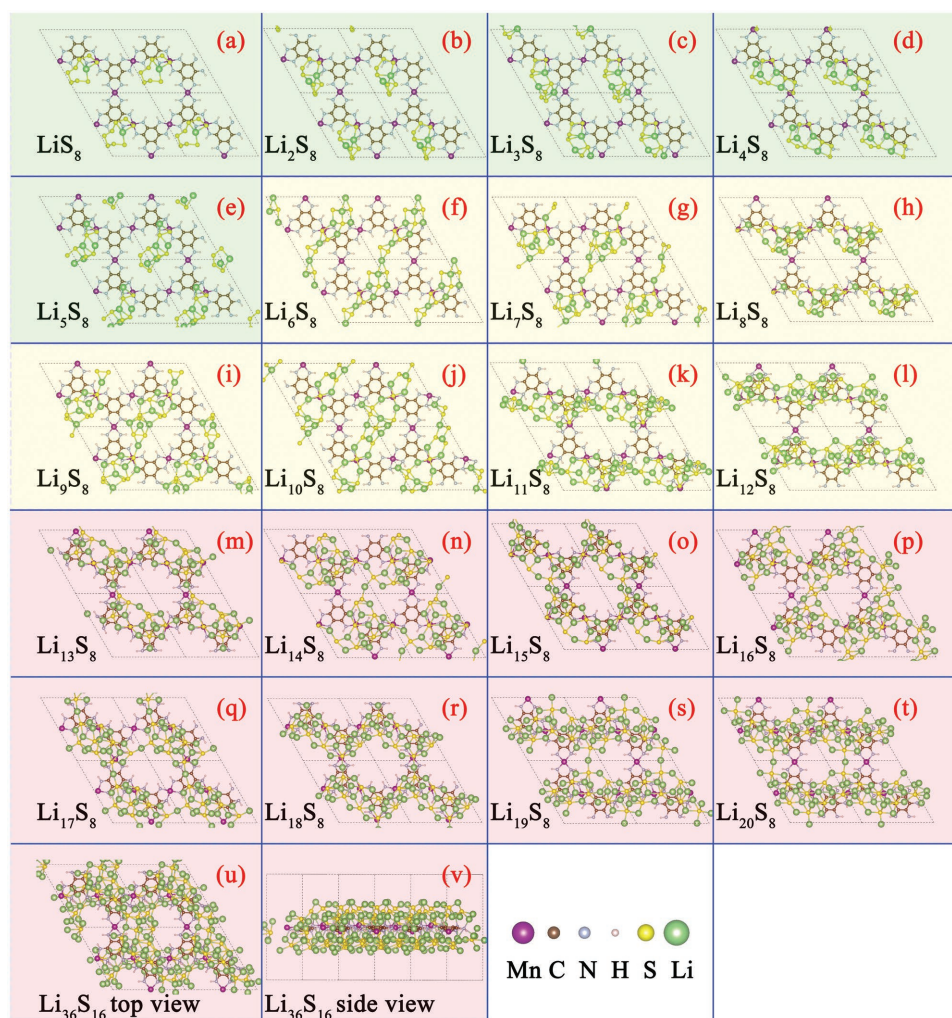


**Figure 4.** The optimized stable structure of  $\text{Li}_x\text{S}_y$  adsorbed on Mn-HAB-CP obtained via genetic algorithm global search. The side views of these structures are shown in Figure S3 in the Supporting Information. The isolated, linear, and meshed  $\text{Li}_x\text{S}_y$  are distinguished by green, yellow, and red background color, respectively.

materials for battery design. This linear behavior only bends a little when the number of Lithium atom increases to 19 and 20. The overall the total formation energy of  $\text{Li}_{20}\text{S}_8$  on Mn-HAB-CP in the solvent is  $-33.65$  eV. This value reaches to  $-65.67$  eV when we add another  $\text{Li}_{16}\text{S}_8$  cluster on the other side of Mn-HAB-CP. The energy density of  $\text{Li}_x\text{S}_y$  on the Mn-HAB-CP with solvent effects at different lithiation stages are shown in the Figure 5b. The energy density is  $310$  Wh  $\text{kg}^{-1}$  with only five lithium added ( $\text{Li}_5\text{S}_8$ ). With ten lithium added, the energy density is  $565$  Wh  $\text{kg}^{-1}$ , which is comparable with the state-of-the-art Li-S value obtained in experiment.<sup>[37]</sup> The energy density increase to  $1012$  Wh  $\text{kg}^{-1}$  when only one side of the Mn-HAB-CP is fully loaded with  $\text{Li}_{20}\text{S}_8$ , and the value further reach  $1395$  Wh  $\text{kg}^{-1}$  if both side are fully loaded (Mn-HAB-CP- $\text{Li}_{36}\text{S}_{16}$ ).

We next study the ability of the system to prevent the dissolution of Li-polysulfide. As shown in Figure 3, the binding energy of the  $\text{Li}_2\text{S}_y$  and Mn-HAB-CP are all negative in the solvent, which means the Mn-HAB-CP itself can absorb the isolated  $\text{Li}_2\text{S}_y$  in the solvent. However, if we propose to use Mn-HAB-CP-

$\text{S}_8$  or Mn-HAB-CP- $2\text{S}_8$  as the starting electrode and gradually lithiated the system, a more relevant question is whether some  $\text{Li}_2\text{S}_y$  cluster can be separated from the  $\text{Li}_x\text{S}_8^*$  or  $\text{Li}_x2\text{S}_8^*$  system and to be dissolved in the solvent. Due to the large number of possible systems and configurations, we have used the  $\text{Li}_{10}\text{S}_8^*$  and  $\text{Li}_{20}\text{S}_8^*$  as two presentative systems to study the dissolution stability. Some of the results are shown in Table 1. Here, we have focused on  $\text{Li}_2\text{S}_8$ ,  $\text{Li}_2\text{S}_6$ , and  $\text{Li}_2\text{S}_4$  molecules since they can be dissolved in the solvent. We see that, for  $1/2$   $\text{Li}_2\text{S}_6$  and  $1/2$   $\text{Li}_2\text{S}_4$  from  $\text{Li}_{10}\text{S}_8^*$  unit, the dissolution energy is slightly negative,  $-0.23$  and  $-0.49$  eV indicating that  $\text{Li}_{10}\text{S}_8^*$  is thermodynamically unstable against the dissolution. On the other hand, the dissolution energy is positive for all the other cases. In particular, the dissolution energy is extremely large for the case of one  $\text{Li}_2\text{S}_8$  molecule separated from two  $\text{Li}_{20}\text{S}_8^*$ . This is because what left behind  $\text{Li}_{19}\text{S}_4^*$  is a rather high-energy structure with too many lithium atoms but a small number of S atoms. We do caution that the dissolution can be a complicated process with many more possible configurations than the one considered here. In future, more detailed and comprehensive studies are

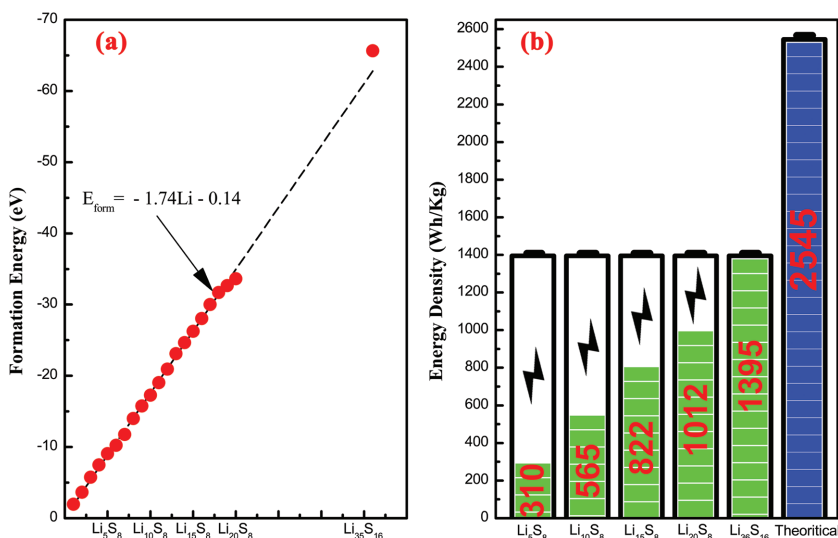


**Figure 5.** a) The overall formation energy of  $\text{Li}_x\text{S}_y$  on Mn-HAB-CP as a function of the number of Li in the solvent (in red color). The fit equations are plotted in black dash-dot lines. b) The energy density of  $\text{Li}_x\text{S}_y$  on the Mn-HAB-CP with solvent effects at different lithiation stages.

necessary. For the small negative dissolution energy cases, we also note that such energy is much smaller than the original Li-S battery, where the  $\text{Li}_2\text{S}_y$  cluster for ( $4 \leq y \leq 8$ ) has to be dissolved into the solvent in order for the lithiation process to continue. In another word, the dissolved state is one step in its lithiation process, and the dissolution is necessary in order to reach the final reduction result (and it also serves as a way to conduct the electric current). In our case, the situation is different. Even though thermodynamically it is not stable against the dissolution in the early stage of the lithiation, it is stable in the later stage of the lithiation, and in order to carry out the discharge at a constant voltage, the intermediate states do not need to be dissolved. This means the kinetic process might be very different from the original Li-S design. Nevertheless, this is an important question worth further study in the future. Other improvements might be possible to enhance the stability, for example, using other transition metal, e.g., V, to replace Mn to have a larger binding energy with S. Perhaps longtime molecular dynamics simulation can also be used to directly monitor the behavior of discharging process.

As discussed in the introduction, conductivity is another critical issue for a good cathode in Li-S battery. We have shown in Figure 1b that pristine Mn-HAB-CP is metallic in the vacuum. The electronic properties can change in solution or after it absorbs Li-S clusters. The Figure 6 presents the band structure

**Table 1.** The separation energies of Mn-HAB-CP- $\text{Li}_x\text{S}_y$  ( $\text{Li}_x\text{S}_y^*$ ) into dissolved  $\text{Li}_2\text{S}_y$  and the remaining Mn-HAB-CP bounded cluster. The total energies of Mn-HAB-CP- $\text{Li}_{10}\text{S}_8$  and Mn-HAB-CP- $\text{Li}_{20}\text{S}_8$  are set to be zero.

$\text{Li}_{10}\text{S}_8^*$	$\text{Li}_9\text{S}_4^*+1/2\text{Li}_2\text{S}_8$	$\text{Li}_9\text{S}_5^*+1/2\text{Li}_2\text{S}_6$	$\text{Li}_9\text{S}_6^*+1/2\text{Li}_2\text{S}_4$
0	0.59	-0.23	-0.49
$\text{Li}_{20}\text{S}_8^*$	$\text{Li}_{19}\text{S}_4^*+1/2\text{Li}_2\text{S}_8$	$\text{Li}_{19}\text{S}_5^*+1/2\text{Li}_2\text{S}_6$	$\text{Li}_{19}\text{S}_6^*+1/2\text{Li}_2\text{S}_4$
0	13.86	10.31	6.24

\*: Mn-HAB-CP.

of various  $\text{Li}_x\text{S}_y^*$  in the solvent. With  $\text{Li}_5\text{S}_8$  on the Mn-HAB-CP, the system is metallic. When  $\text{Li}_{10}\text{S}_8$  is absorbed on Mn-HAB-CP, a small band gap of 0.28 eV is open up. This small gap is closed slowly as the lithium number increase. In case of  $\text{Li}_{20}\text{S}_8$ , the band gap is only 0.07 eV. In addition, with  $\text{Li}_x\text{S}_y$  clusters loading on both side of Mn-HAB-CP ( $\text{Li}_{36}\text{S}_{16}^*$ ), the system is metallic. In the real experimental situation, the Li-S clusters will be loaded on both sides of Mn-HAB-CP simultaneously. We expect the system is always metallic or very close to metal.

In above, we have addressed two of the three challenges facing Li-S battery, the dissolution of Li-polysulfide, and the insulating nature of the cathode material. Another challenge is the volume expansion. So far, we have only studied systems with Li-S absorbed on the two sides of Mn-HAB-CP. The system is essential 2D. If the system is always 2D, its volumetric capacity will be rather small. One approach to solve this problem is to construct

a 3D porous system, or mix Mn-HAB-CP 2D flakes with other conductive binders like carbon black. Here, we briefly introduce a design which sandwiches the Li-S layer with two layers of Mn-HAB-CP. As a matter of fact, it can be stacked up into a periodic 3D system with artificial layer structure. Such a design not only can increase the volumetric capacity and it also has a potential to prevent the dissolution problem discussed above. While a full exploration of such a system deserves a separated detailed study, especially for the ability to diffuse the Li into such a 3D structure, here we like to focus on one interesting issue: the volume expansion of the system upon lithiation. As shown in Figure 7, in the starting electrode Mn-HAB-CP- $\text{S}_8$ , the Mn-HAB-CP/ Mn-HAB-CP interlayer distance is 6.34 Å (see Figure 7b). However, when 20 lithium atoms are added to each Mn-HAB-CP- $\text{S}_8$ , making it Mn-HAB-CP- $\text{Li}_{20}\text{S}_8$ , the Mn-HAB-CP/ Mn-HAB-CP distance only increases to 6.51 Å. Thus, there is only 2.7% lattice constant increase in the z-direction. This is rather remarkable and the distance increase is similar to that of the LIB battery.

## 4. Conclusion

The 2D hexaaminobenzene-based coordination polymers have been investigated as Li-S battery cathode via DFT calculation in combination with in-house developed charge polarized solvent model and genetic algorithm global structure search algorithm. The parameters of the solvent model are fixed by comparing the  $\text{Li}_2\text{S}_y$  (for  $y = 4, 6, 8$ ) molecule energies in the solvent with the experimental charging/discharging voltages. For a given chemical formula compound, the genetic algorithm is used to find the minimum energy configuration. Through our theoretical studies, we have the following conclusions: 1) The pristine Mn-HAB-CP will absorb  $\text{Li}_2\text{S}_y$  molecules from the solvent, and the transition metal will also absorb  $\text{S}_8$  molecule to its surface to be bonded with the Mn atom; 2) with more lithium

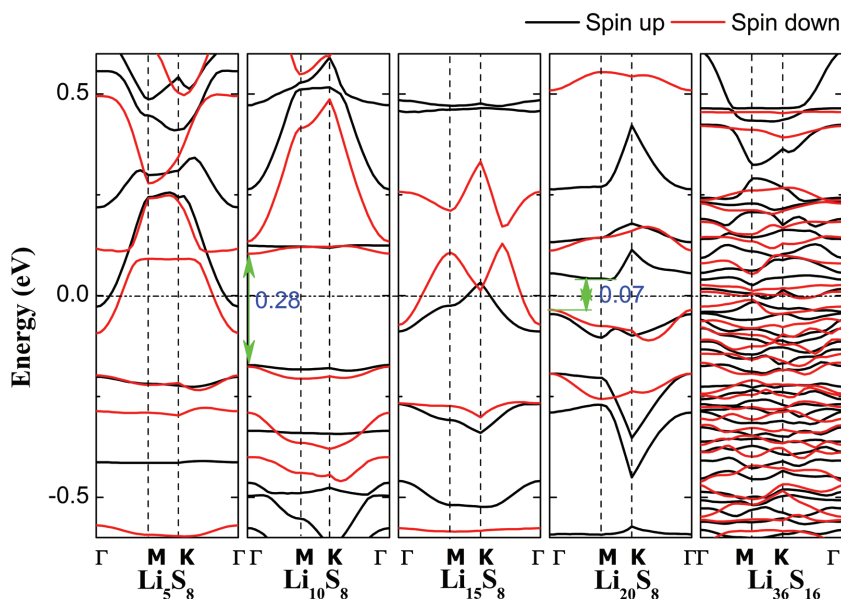


**Figure 6.** The band structures of Mn-HAB-CP with  $\text{Li}_2\text{S}_\gamma$  clusters ( $\text{Li}_\gamma\text{S}_\gamma^*$ ) along the high symmetry  $\Gamma$ -K-M- $\Gamma$  directions in the solvent. The associated Brillouin zone is shown in Figure 1. The Fermi energy in the band structure is at 0.

atoms added to the Mn-HAB-CP- $\text{S}_8$  or Mn-HAB-CP- $2\text{S}_8$  system, the  $\text{S}_8$  will be broken into smaller and smaller pieces. Different structure patterns will be formed, from parallel wires eventually to Li-S alternating layer structures resemble that in crystal  $\text{Li}_2\text{S}$ . In the fully lithiated structures, there is no more Mn-S bond, instead, Li layer will be first bound with the Mn-HAB-CP, followed by the S layer. Li atoms are bonded with the two-coordinated edge N atoms; 3) the lithiation formation energy is almost a straight line of the number of Li atoms, indicating a constant voltage of about 1.74 V for the whole charge/discharge process. The final energy density for the Mn-HAB-CP- $\text{Li}_{20}\text{S}_8$ - $\text{Li}_{16}\text{S}_8$  final product is  $1395 \text{ Wh kg}^{-1}$ ;

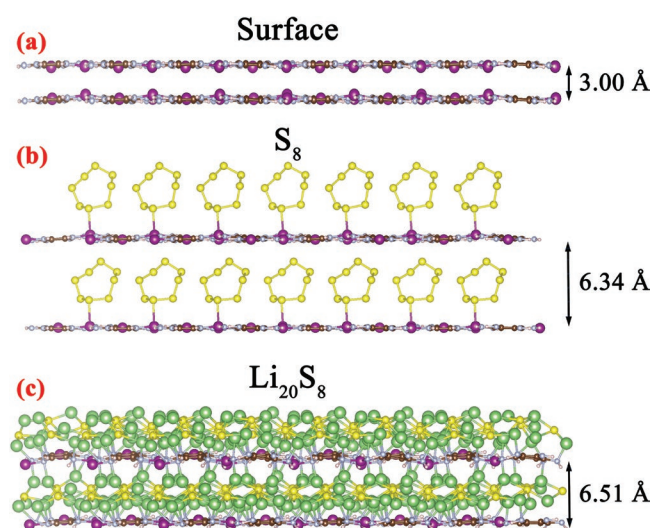


**Figure 7.** The interlayer distance of two layers of a) Mn-HAB-CP,  $\text{S}_8$  loaded b) Mn-HAB-CP, and  $\text{Li}_{20}\text{S}_8$  loaded Mn-HAB-CP (half charged). c) The color codes of elements refer to Figure 4.

4) while for the final product Mn-HAB-CP- $\text{Li}_{20}\text{S}_8$ , the system is thermodynamically stable against dissolution/separation of  $\text{Li}_2\text{S}_\gamma$  ( $\gamma = 4, 6, 8$ ) molecules, the system could be thermodynamically unstable at the intermediate stage as for Mn-HAB-CP- $\text{Li}_{10}\text{S}_8$ . Further studies are needed to address this issue, especially for the kinetic path of the molecule dissolution, or to find ways to increase the S-substrate-binding energy; 5) the electrode is metallic throughout the charging/discharge process, hence solving the insulating problem in the original Li-S battery set-up; and 6) a sandwiched design is proposed, which changes the 2D electrode into a 3D system, hence provides sufficient volumetric capacity. It is found that the vertical expansion of the system after full lithiation is only 3%, rivals that of the LIB systems. Besides, such design could also provide a kinetic barrier for  $\text{Li}_2\text{S}_\gamma$  dissolution. All our findings show that Mn-HAB-CP could be a potentially promising Li-S cathode material, and offer a new computational framework to investigate the Li-S battery and other processed with solvent effects.

## Supporting Information

Supporting Information is available from the Wiley Online Library or from the author.

## Acknowledgements

This work was supported by the Assistant Secretary for Energy Efficiency and Renewal Energy of the U.S. Department of Energy under the Battery Materials Research (BMR) program. The theoretical work in this research used the resources of the National Energy Research Scientific Computing Center (NERSC) that was supported by the Office of Science of the U. S. Department of Energy. This work also used the computational resource of the Oak Ridge Leadership Computing Facility at the Oak Ridge National Laboratory under the Innovative and Novel Computational Impact on Theory and Experiment project.

## Conflict of Interest

The authors declare no conflict of interest.

## Keywords

2D hexaaminobenzene-based coordination polymers, cathode materials, Li-S batteries

Received: June 11, 2018  
Published online: July 25, 2018

- [1] J. B. Goodenough, K.-S. Park, *J. Am. Chem. Soc.* **2013**, *135*, 1167.  
[2] Y. Liu, G. Zhou, K. Liu, Y. Cui, *Acc. Chem. Res.* **2017**, *50*, 2895.

- [3] P. G. Bruce, S. A. Freunberger, L. J. Hardwick, J.-M. Tarascon, *Nat. Mater.* **2011**, *11*, 19.
- [4] a) A. Manthiram, Y. Fu, Y.-S. Su, *Acc. Chem. Res.* **2013**, *46*, 1125; b) R. Xu, J. Lu, K. Amine, *Adv. Energy Mater.* **2015**, *5*, 1500408.
- [5] N. Imanishi, O. Yamamoto, *Mater. Today* **2014**, *17*, 24.
- [6] a) Z. Sun, J. Zhang, L. Yin, G. Hu, R. Fang, H.-M. Cheng, F. Li, *Nat. Commun.* **2017**, *8*, 14627; b) L. Zhang, D. Sun, J. Feng, E. J. Cairns, J. Guo, *Nano Lett.* **2017**, *17*, 5084; c) A. Manthiram, Y. Fu, S.-H. Chung, C. Zu, Y.-S. Su, *Chem. Rev.* **2014**, *114*, 11751.
- [7] a) X. Ji, K. T. Lee, L. F. Nazar, *Nat. Mater.* **2009**, *8*, 500; b) Y. Li, K. K. Fu, C. Chen, W. Luo, T. Gao, S. Xu, J. Dai, G. Pastel, Y. Wang, B. Liu, J. Song, Y. Chen, C. Yang, L. Hu, *ACS Nano* **2017**, *11*, 4801; c) T. Hou, X. Chen, H. Peng, J. Huang, B. Li, Q. Zhang, B. Li, *Small* **2016**, *12*, 3283.
- [8] S. Zheng, Y. Wen, Y. Zhu, Z. Han, J. Wang, J. Yang, C. Wang, *Adv. Energy Mater.* **2014**, *4*, 1400482.
- [9] G. Zhou, J. Sun, Y. Jin, W. Chen, C. Zu, R. Zhang, Y. Qiu, J. Zhao, D. Zhuo, Y. Liu, X. Tao, W. Liu, K. Yan, H. R. Lee, Y. Cui, *Adv. Mater.* **2017**, *29*, 1603366.
- [10] Y. Li, K. Yan, H.-W. Lee, Z. Lu, N. Liu, Y. Cui, *Nat. Energy* **2016**, *1*, 15029.
- [11] a) H. Wang, T. Zhou, D. Li, H. Gao, G. Gao, A. Du, H. Liu, Z. Guo, *ACS Appl. Mater. Interfaces* **2017**, *9*, 4320; b) Z. Yuan, H.-J. Peng, T.-Z. Hou, J.-Q. Huang, C.-M. Chen, D.-W. Wang, X.-B. Cheng, F. Wei, Q. Zhang, *Nano Lett.* **2016**, *16*, 519.
- [12] Q. Pang, D. Kundu, L. F. Nazar, *Mater. Horiz.* **2016**, *3*, 130.
- [13] R. Demir-Cakan, M. Morcrette, F. Nouar, C. Davoisne, T. Devic, D. Gonbeau, R. Dorninko, C. Serre, G. Férey, J.-M. Tarascon, *J. Am. Chem. Soc.* **2011**, *133*, 16154.
- [14] L. Wang, Y. Han, X. Feng, J. Zhou, P. Qi, B. Wang, *Coord. Chem. Rev.* **2016**, *307*, 361.
- [15] N. Lahiri, N. Lotfizadeh, R. Tsuchikawa, V. V. Deshpande, J. Louie, *J. Am. Chem. Soc.* **2017**, *139*, 19.
- [16] G. Gao, E. R. Waclawik, A. Du, *J. Catal.* **2017**, *352*, 579.
- [17] D. Feng, T. Lei, M. R. Lukatskaya, J. Park, Z. Huang, M. Lee, L. Shaw, S. Chen, A. A. Yakovenko, A. Kulkarni, J. Xiao, K. Fredrickson, J. B. Tok, X. Zou, Y. Cui, Z. Bao, *Nat. Energy* **2018**, *3*, 30.
- [18] a) F. Li, J. Zhao, *Phys. Chem. Chem. Phys.* **2018**, *20*, 4005; b) F. Li, J. Zhao, *ACS Appl. Mater. Interfaces* **2017**, *9*, 42836; c) L.-C. Yin, J. Liang, G.-M. Zhou, F. Li, R. Saito, H.-M. Cheng, *Nano Energy* **2016**, *25*, 203.
- [19] T. A. Pham, M. Govoni, R. Seidel, S. E. Bradforth, E. Schwegler, G. Galli, *Sci. Adv.* **2017**, *3*.
- [20] G. Zhou, H. Tian, Y. Jin, X. Tao, B. Liu, R. Zhang, Z. W. Seh, D. Zhuo, Y. Liu, J. Sun, J. Zhao, C. Zu, D. S. Wu, Q. Zhang, Y. Cui, *Proc. Natl. Acad. Sci. USA* **2017**, *114*, 840.
- [21] a) W. Jia, Z. Cao, L. Wang, J. Fu, X. Chi, W. Gao, L.-W. Wang, *Comput. Phys. Commun.* **2013**, *184*, 9; b) W. Jia, J. Fu, Z. Cao, L. Wang, X. Chi, W. Gao, L.-W. Wang, *J. Comput. Phys.* **2013**, *251*, 102.
- [22] J. P. Perdew, K. Burke, M. Ernzerhof, *Phys. Rev. Lett.* **1996**, *77*, 3865.
- [23] J. P. Perdew, M. Ernzerhof, K. Burke, *J. Chem. Phys.* **1996**, *105*, 9982.
- [24] S. Grimme, *J. Comput. Chem.* **2006**, *27*, 1787.
- [25] S. L. Dudarev, G. A. Botton, S. Y. Savrasov, C. J. Humphreys, A. P. Sutton, *Phys. Rev. B* **1998**, *57*, 1505.
- [26] J. Tomasi, B. Mennucci, R. Cammi, *Chem. Rev.* **2005**, *105*, 2999.
- [27] C. Dupont, O. Andreussi, N. Marzari, *J. Chem. Phys.* **2013**, *139*, 214110.
- [28] R. E. Skyner, J. L. McDonagh, C. R. Groom, T. van Mourik, J. B. O. Mitchell, *Phys. Chem. Chem. Phys.* **2015**, *17*, 6174.
- [29] X. Chen, H.-J. Peng, R. Zhang, T.-Z. Hou, J.-Q. Huang, B. Li, Q. Zhang, *ACS Energy Lett.* **2017**, *2*, 795.
- [30] a) D. Ghosh, A. Roy, R. Seidel, B. Winter, S. Bradforth, A. I. Krylov, *J. Phys. Chem. B* **2012**, *116*, 7269; b) R. S. Assary, L. A. Curtiss, J. S. Moore, *J. Phys. Chem. C* **2014**, *118*, 11545.
- [31] C. Barchasz, F. Molton, C. Duboc, J.-C. Leprêtre, S. Patoux, F. Alloin, *Anal. Chem.* **2012**, *84*, 3973.
- [32] a) J. Wu, L.-W. Wang, *J. Mater. Chem. A* **2018**, *6*, 2984; b) N. N. Rajput, V. Murugesan, Y. Shin, K. S. Han, K. C. Lau, J. Chen, J. Liu, L. A. Curtiss, K. T. Mueller, K. A. Persson, *Chem. Mater.* **2017**, *29*, 3375.
- [33] G. Yang, S. Shi, J. Yang, Y. Ma, *J. Mater. Chem. A* **2015**, *3*, 8865.
- [34] B. Wang, S. M. Alhassan, S. T. Pantelides, *Phys. Rev. Appl.* **2014**, *2*, 034004.
- [35] Z. W. Seh, J. H. Yu, W. Li, P.-C. Hsu, H. Wang, Y. Sun, H. Yao, Q. Zhang, Y. Cui, *Nat. Commun.* **2014**, *5*, 5017.
- [36] S. Darby, T. V. Mortimer-Jones, R. L. Johnston, C. Roberts, *J. Chem. Phys.* **2002**, *116*, 1536.
- [37] Y. Yang, M. T. McDowell, A. Jackson, J. J. Cha, S. S. Hong, Y. Cui, *Nano Lett.* **2010**, *10*, 1486.